Field Effect Control of Surface Charge Property and Electroosmotic Flow in Nanofluidics

ARTICLE *in* THE JOURNAL OF PHYSICAL CHEMISTRY C · FEBRUARY 2012

Impact Factor: 4.77 · DOI: 10.1021/jp211496b

5 AUTHORS, INCLUDING:

Li-Hsien Yeh
National Yunlin University of Science and Tec…
63 PUBLICATIONS **717** CITATIONS
SEE PROFILE

Shizhi Qian
Old Dominion University
156 PUBLICATIONS **2,513** CITATIONS
SEE PROFILE

THE JOURNAL OF PHYSICAL CHEMISTRY C

Article

pubs.acs.org/JPCC

Field Effect Control of Surface Charge Property and Electroosmotic Flow in Nanofluidics

Li-Hsien Yeh,[†,‡,∥] Song Xue,[†,∥] Sang Woo Joo,[§] Shizhi Qian,*[,†,§] and Jyh-Ping Hsu*[,‡]

[†]Institute of Micro/Nanotechnology, Old Dominion University, Norfolk, Virginia 23529, United States

[‡]Department of Chemical Engineering, National Taiwan University, Taipei, 10617, Taiwan

[§]School of Mechanical Engineering, Yeungnam University, Gyongsan 712-719, South Korea

ABSTRACT: The surface charge property of nanofluidic devices plays an essential role in electrokinetic transport of ions, fluids, and particles in them. The nanofluidic field effect transistor (FET), referring to a nanochannel embedded with an electrically controllable gate electrode, provides a simple way to rapidly regulate its surface charge property, which in turn controls the electrokinetic transport phenomena within the nanochannel. In this study, approximate analytical expressions are derived for the first time to estimate the surface-charge property and electroosmotic flow (EOF) in charge-regulated nanochannels tuned by the nanofluidic FET and are validated by comparing their predictions to the existing experimental data available from the literature. The control of the surface charge property as well as the EOF by the nanofluidic FET depends on the pH and ionic concentration of the aqueous solution.

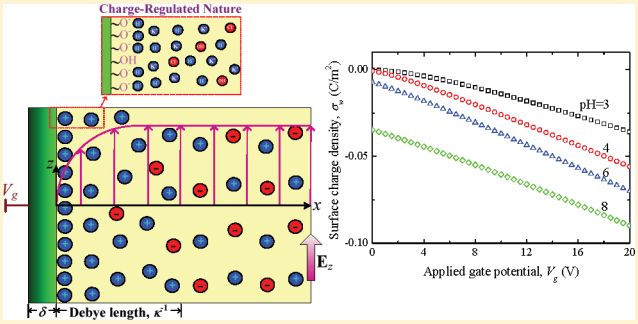

1. INTRODUCTION

With recent advances in nanofabrication techniques[1−3] and growing interest in sensing single molecules by nanofluidic devices,[3−6] active control of the transport of ions, fluids, and (bio)particles through biological and/or synthetic nanochannels has attracted significant attention over the past decade. It is generally accepted that the electrokinetic transport of ions, fluids, and particles in nanofluidic devices highly depends on the surface charge property of the nanochannel wall, which is in contact with the aqueous solution, especially when the thickness of the electrical double layer (EDL) is comparable to the nanochannel width.[7] Several attempts have been made on the modulation of the surface charge property of the nanochannels, including, for example, adjusting the pH and chemicals in the aqueous solution[8−10] as well as surface modification via chemically or physically grafting functional groups to the channel wall.[11,12] However, the above passive methods lack the flexibility and capability of rapidly tuning the surface charge on the nanopore wall.

Recently, a fluidic field effect transistor (FET),[13,14] referring to the micro/nanochannel embedded with an electrically controllable gate electrode, has been demonstrated to rapidly tune the surface charge condition and accordingly the magnitude and direction of the electroosmotic flow (EOF) in micro/nanofluidic devices.[13−25] In the field effect control of the surface potential, an electric bias called gate potential is applied to the gate electrode fabricated along the outer surface of the dielectric channel wall. The gate electrode and the liquid inside the micro/nanochannel are separated by an electrically insulating layer, which is made of dielectric material such as silicon dioxide (SiO_2). The surface of the gated dielectric channel wall in contact with the aqueous solution is often assumed to bear a negative surface charge according to its dissociation/association constant. Depending upon different manufacturing processes, the point of zero charge (PZC) for SiO_2 ranges from 2 to 3.5.[26] Since the silanol groups (Si−OH) on the SiO_2 surface are deprotonated to produce $Si-O^-$ when the pH is above the PZC, the SiO_2 surface in contact with an aqueous solution is typically negatively charged, and its surface charge density depends on pH of the liquid phase.[27] Previous studies, however, assume that the gated solid/liquid interface bears a constant surface charge density[21,23,24] or even uncharged[17,19,20,22,25] without considering the pH effect. This assumption is inaccurate and unrealistic because the surface charge density at that interface largely depends on the pH of the liquid phase, the ionic concentration, and the applied gate potential in gated FET control systems. Therefore, a new model, which takes into account the effects of the pH of the aqueous solution, the site number density, and dissociation/association constants of the functional groups on the dielectric layer surface, is highly desirable for elucidating the detailed mechanism of the micro/nanofluidic FET to tune the electrokinetic phenomena in micro/nanofluidic devices and is the main subject of this study.

In the present study, a charge-regulated model is used for the first time to investigate the surface charge property and EOF in

Received: November 29, 2011
Revised: January 10, 2012
Published: January 17, 2012

   dx.doi.org/10.1021/jp211496b | J. Phys. Chem. C 2012, 116, 4209−4216

a gated nanofluidic channel by FET. Approximate expressions, including both analytical and implicit solutions, for predicting the zeta potential and EOF velocity as functions of the applied gate potential, pH, and ionic concentrations of the electrolyte, and the properties of the dielectric layer (i.e., permittivity and thickness) are derived for the first time. The models are further validated by existing experimental data available from the literature. The model developed should be very useful for understanding and designing the FET-based micro/nanofluidic devices.

2. THEORETICAL ANALYSIS

We consider a steady EOF of an aqueous electrolyte solution of relative permittivity ε_f within a nanofluidic field effect transistor, as schematically shown in Figure 1a. The FET consists of a gate

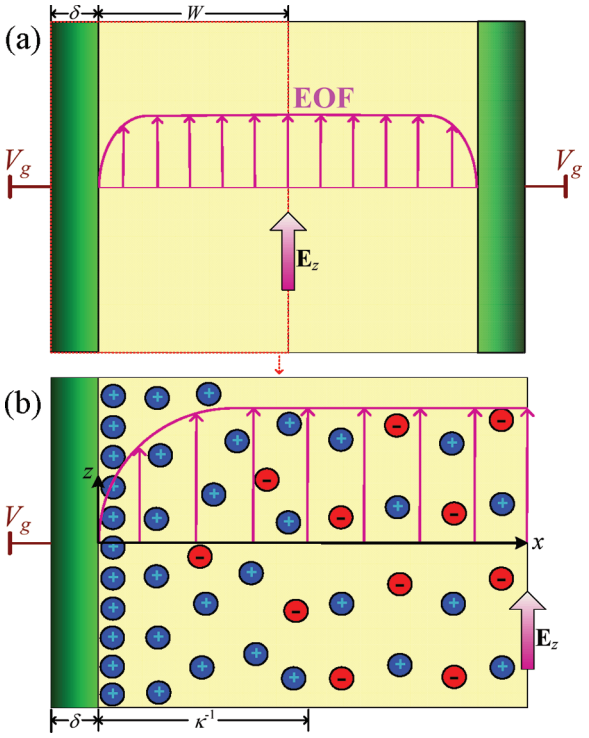

Figure 1. (a) Schematic illustrating the regulation of the electro-osmotic flow by a nanofluidic field effect transistor (FET). (b) Schematic representation of the problem under consideration.

electrode patterned on the outer surface of a dielectric layer of thickness, δ, and relative permittivity, ε_d. A uniform electric field, $\mathbf{E}_z$, of strength E_z is applied tangential to the gated nanochannel wall, generating steady EOF parallel to the channel wall. A gate potential, V_g, is imposed on the gate electrode to tune the surface potential of the inner channel wall and accordingly controls the EOF within the nanochannel.

We use a Cartesian coordinate system (x, z) with the origin located at the solid/liquid interface. The x- and z-axes are, respectively, perpendicular and parallel to the planar channel wall in contact with the aqueous solution. We assume (i) the liquid is incompressible, and the flow is in the creeping flow regime considering that typical Reynolds numbers of EOF in nanofluidics are much smaller than 1; (ii) the effect of the Stern layer adjacent to the channel wall is neglected so that the electric potential at the solid/liquid interface represents the zeta potential of the planar surface, ζ; (iii) the planar surface of the dielectric material in contact with the aqueous solution is of charge-regulated nature[28] and bears a uniform surface charge density of σ_w along the z-direction; (iv) the EDLs of the two opposite channel walls are not overlapped so that the present problem can be simplified to the case of a planar FET in contact with a semi-infinite aqueous electrolyte solution, as schematically shown in Figure 1b. This assumption is valid only if the Debye length (or the EDL thickness, κ^{-1}) is much smaller than the half width of the nanochannel, $\lambda_D = \kappa^{-1} \ll W$, and holds under most experimental conditions. For example, the bulk electrolyte concentration in experiments is typically in the range of 1−1000 mM,[10,17,23,24,29] and the Debye length accordingly ranges from 9.6 to 0.3 nm,[7] which is very thin compared to most W in experiments. With the above assumptions, the distributions of the electric potential, the ionic concentrations, and the flow field of the liquid are uniform along the z-direction. The analysis under consideration can be simplified to one-dimensional, which is perpendicular to the channel wall.

2.1. Full Multi-Ion Model. For a general electrolyte solution containing N types of ionic species, the electric potentials inside and outside the dielectric channel wall (regions I and II) are, respectively, governed by the Laplace equation and the Poisson−Boltzmann equation[19,30]

$$\frac{d^2\phi}{dx^2} = 0 \text{ in region I} \tag{1}$$

and

$$\frac{d^2\psi}{dx^2} = -\frac{\rho_e}{\varepsilon_f\varepsilon_0} = -\frac{1}{\varepsilon_f\varepsilon_0}\sum_{i=1}^{N} Fz_iC_{i0}\exp\left(-\frac{z_iF\psi}{RT}\right) \text{ in region II} \tag{2}$$

In the absence of the pressure gradient in the z-direction, the steady EOF velocity, u, in the z-direction is governed by

$$\frac{d^2u}{dx^2} = -\frac{1}{\mu}\rho_eE_z \text{ in region II} \tag{3}$$

In the above, ϕ is the electric potential inside the dielectric layer; ψ is the potential within the liquid; ε_0 is the absolute permittivity of vacuum; ρ_e is the net space charge density; z_i and C_{i0} are the valence and the bulk concentration of the ith ionic species, respectively; and F, R, T, and μ are the Faraday constant, the universal gas constant, the absolute temperature, and the dynamical viscosity of the electrolyte solution, respectively.

A constant gate potential, V_g, is imposed on the gate electrode at $x = -\delta$, and we further assume that the planar channel wall in contact with the aqueous solution is nonslip. The boundary conditions associated with eqs 1−3 are

$$\phi = V_g \text{ at } x = -\delta \tag{4}$$

$$\phi = \psi \cong \zeta \text{ at } x = 0 \tag{5}$$

$$\varepsilon_0\varepsilon_f\frac{d\psi}{dx} - \varepsilon_0\varepsilon_d\frac{d\phi}{dx} = -\sigma_w \text{ at } x = 0 \tag{6}$$

dx.doi.org/10.1021/jp211496b | J. Phys. Chem. C 2012, 116, 4209−4216

$$\psi = 0 \text{ and } \frac{d\psi}{dx} = 0 \text{ as } x \to \infty \tag{7}$$

$$u = 0 \text{ at } x = 0 \tag{8}$$

and

$$\frac{du}{dx} = 0 \text{ as } x \to \infty \tag{9}$$

Equations 5 and 6 imply that the electric potential is continuous at the solid/liquid interface, but the electric field is not due to the discontinuity of the electric permittivities at the interface, where the electric field satisfies the Gauss law.

The surface charge density, σ_w, in eq 6 will be determined by the following charge-regulation model. Typically, due to the protonation/deprotonation surface reactions occurring on the dissociably functional groups of the solid/liquid interface, the dielectric material surface reveals a charge-regulated nature when it is in contact with an aqueous solution. Therefore, the surface charge property of the FET solid/liquid interface depends on the solution properties such as its pH and ionic concentration. To account for the charge regulation, we assume that the following two main dissociation/association reactions with equilibrium constants K_A and K_B occur on that solid/liquid interface

$$MOH \leftrightarrow MO^- + H^+ \tag{10}$$

and

$$MOH + H^+ \leftrightarrow MOH_2^+ \tag{11}$$

At the equilibrium state, one has

$$K_A = \frac{N_{MO^-}[H^+]_s}{N_{MOH}} \tag{12}$$

and

$$K_B = \frac{N_{MOH_2^+}}{N_{MOH}[H^+]_s} \tag{13}$$

In the above, N_{MOH}, N_{MO^-}, and $N_{MOH_2^+}$ are the surface site densities of MOH, MO^-, and MOH_2^+, respectively, and $[H^+]_s$ is the concentration of H^+ ions at the solid/liquid interface that follows the Boltzmann distribution, $[H^+]_s = [H^+]_0 \exp[(F\zeta)/(RT)]$. The total number site density of MOH molecules on the solid/liquid interface is $N_{total} = N_{MOH} + N_{MO^-} + N_{MOH_2^+}$. On the basis of eqs 12 and 13, the relation of $\sigma_w = -F(N_{MO^-} - N_{MOH_2^+})$ gives

$$\sigma_w = -FN_{total}\left\{\frac{K_A - K_B\left[[H^+]_0\exp\left(-\frac{F\zeta}{RT}\right)\right]^2}{K_A + [H^+]_0\exp\left(-\frac{F\zeta}{RT}\right) + K_B\left[[H^+]_0\exp\left(-\frac{F\zeta}{RT}\right)\right]^2}\right\} \tag{14}$$

where $[H^+]_0$ is the bulk concentration of H^+ ions and is related to the pH value of the bulk liquid by $pH = -\log([H^+]_0)$. In contrast to the previous studies with a constant surface charge density,[17,19,20,22,25] this study handles the surface charge density as a part of the solution for given pH value and physiochemical properties of the dielectric material.

2.2. Approximation Model. One has to numerically solve the above eqs 1−3 if the total number of ionic species in the solution is more than 2 (i.e., $N > 2$). When the concentration of the background electrolyte is much higher than the concentrations of the ions H^+ and OH^-, the contributions of the ions H^+ and OH^- to the net charge density, ρ_e, in eqs 2 and 3 can be neglected. When the above condition holds and the background electrolyte only contains binary symmetric caitons and anions such as K^+ and Cl^-, eqs 2 and 3 can be rewritten as

$$\frac{d^2\left(\frac{zF\psi}{RT}\right)}{dx^2} = \kappa^2 \sinh\left(\frac{zF\psi}{RT}\right) \text{ in region II} \tag{15}$$

and

$$\frac{d^2u}{dx^2} = \frac{\varepsilon_0\varepsilon_f E_z}{\mu}\frac{d^2\psi}{dx^2} \text{ in region II} \tag{16}$$

where $z = z_1 = -z_2$, $C_0 = C_{10} = C_{20}$, and $\lambda_D = \kappa^{-1} = (\varepsilon_f\varepsilon_0 RT/2z^2F^2C_0)^{1/2}$ is the Debye length.

Solving eqs 1 and 15 subjected to the boundary conditions, eqs 4−7, we get

$$\phi = (\zeta - V_g)\left(\frac{x}{\delta}\right) + \zeta \tag{17}$$

and

$$\psi = \frac{2RT}{Fz}\ln\left[\frac{1 + \exp(-\kappa x)\tanh\left(\frac{Fz\zeta}{4RT}\right)}{1 - \exp(-\kappa x)\tanh\left(\frac{Fz\zeta}{4RT}\right)}\right] \tag{18}$$

Note that eq 18 is the well-known Gouy−Chapman solution for the planar surface system. By substituting eq 18 into eq 16 and solving the resultant equation subjected to the boundary conditions, eqs 8 and 9, we obtain the relation between the EOF velocity, u, and the zeta potential, ζ

$$u = 4u_r \tanh^{-1}\left[\tanh\left(\frac{Fz\zeta}{4RT}\right)\exp(-\kappa x)\right] - \frac{\varepsilon_0\varepsilon_f E_z\zeta}{\mu} \tag{19}$$

where $u_r = (\varepsilon_0\varepsilon_f E_z/\mu)(RT/Fz)$ is the magnitude of the Smoluchowski electroosmotic velocity with the zeta potential of RT/Fz.

By substituting eqs 14, 17, and 18 into eq 6, we obtain the following implicit equation relating the zeta potential, ζ, to the externally imposed gate potential, V_g, the electric property and thickness of the dielectric layer, ε_d and δ, the physicochemical interface properties of the dielectric layer, K_A, K_B, and N_{total},

dx.doi.org/10.1021/jp211496b | J. Phys. Chem. C 2012, 116, 4209−4216

pH of the solution (pH = $-\log([H^+]_0)$), and κ which depends on the bulk ionic concentration, C_0

$$\frac{2\varepsilon_0\varepsilon_f\kappa RT}{zF}\sinh\left(\frac{Fz\zeta}{2RT}\right)+\varepsilon_0\varepsilon_d\left(\frac{\zeta-V_g}{\delta}\right)=-FN_{total}\left\{\frac{K_A-K_B\left[[H^+]_0\exp\left(-\frac{F\zeta}{RT}\right)\right]^2}{K_A+[H^+]_0\exp\left(-\frac{F\zeta}{RT}\right)+K_B\left[[H^+]_0\exp\left(-\frac{F\zeta}{RT}\right)\right]^2}\right\} \quad (20)$$

One can easily use, for example, MATLAB function *fzero* to determine ζ for giving appropriate values of other parameters. By substituting ζ obtained into eqs 18 and 19, we obtain the spatial distributions of the potential, ψ, and the EOF velocity, u. The surface charge density, σ_w, can then be evaluated by eq 14 based on the obtained ζ.

In general, eq 20 needs to be solved numerically. However, if we consider the case of low surface potential, $\zeta \ll RT/zF$, eqs 14, 18, 19, and 20 can be simplified as

$$\sigma_w=-FN_{total}\left\{\frac{\Phi}{\Omega}+\left(\frac{F\zeta}{RT}\right)\left[\frac{\Pi}{\Omega}+\frac{\Phi([H^+]_0+\Pi)}{\Omega^2}\right]\right\} \quad (21)$$

$$\psi=\zeta\exp(-\kappa x) \quad (22)$$

$$u=\frac{\varepsilon_0\varepsilon_f E_z\zeta}{\mu}[\exp(-\kappa x)-1] \quad (23)$$

and

$$\varepsilon_0\varepsilon_f\kappa\zeta+\varepsilon_0\varepsilon_d\left(\frac{\zeta-V_g}{\delta}\right)=-FN_{total}\left\{\frac{\Phi}{\Omega}+\left(\frac{F\zeta}{RT}\right)\left[\frac{\Pi}{\Omega}+\frac{\Phi([H^+]_0+\Pi)}{\Omega^2}\right]\right\} \quad (24)$$

where $\Omega = K_A + [H^+]_0 + K_B[H^+]_0^2$, $\Phi = K_A - K_B[H^+]_0^2$, and $\Pi = 2K_B[H^+]_0^2$.

Solving eq 24, we obtain

$$\zeta=\frac{-\delta FN_{total}\left(\frac{\Phi}{\Omega}\right)+\varepsilon_0\varepsilon_d V_g}{\varepsilon_0\varepsilon_f\kappa\delta+\varepsilon_0\varepsilon_d+\delta FN_{total}\left(\frac{F}{RT}\right)\left[\frac{\Pi}{\Omega}+\frac{\Phi([H^+]_0+\Pi)}{\Omega^2}\right]} \quad (25)$$

Under the Debye–Hückel approximation (i.e., $\zeta \ll RT/zF$), eq 25 clearly shows that ζ is linearly proportional to the externally imposed gate potential, V_g. It also shows that the degree of the field effect control depends on other parameters such as the surface properties and material of the dielectric layer (i.e., ε_d, δ, K_A, K_B, and N_{total}), pH of the bulk electrolyte (i.e., $[H^+]_0$), and the bulk ionic concentration of the background electrolyte (i.e., C_0). Once ζ is obtained, σ_w, ψ, and u can be easily evaluated from eqs 21, 22 and 23, respectively.

3. RESULTS AND DISCUSSION

3.1. Verification of the Approximation Model. To validate the model for the zeta potential (eqs 20 and 25) derived above and the EOF velocity profile (eqs 19 and 23), we compare the results of the approximate model (Section 2.2) to those of the full multi-ion model (Section 2.1). We consider a monovalent background electrolyte solution, such as KCl with $z = 1$, and the dielectric layer made of silicon dioxide with $\varepsilon_d = 3.9$,[19] $N_{total} = 8 \times 10^{-6}$ mol/m^2, pK_A = 6.8, and pK_B = 1.9.[31] Note that p$K_j = -\log K_j$ (j = A and B). The other relevant physical constants are $\varepsilon_f = 80$, $\varepsilon_0 = 8.854 \times 10^{-12}$ CV^{-1} m^{-1}, R = 8.314 J K^{-1} mol^{-1}, T = 298 K, $\mu = 10^{-3}$ kg m^{-1} s^{-1}, and F = 96 490 C mol^{-1}.

Figure 2 depicts the variations of the zeta potential ζ at various combinations of the pH values, the bulk ionic concentrations, C_0, and the applied gate potentials, V_g. Symbols represent the zeta potential obtained from the implicit eq 20 where only the background electrolyte ions K^+ and Cl^- are considered. Lines represent numerical results obtained from the full multi-ion model considering four types of ions, K^+, Cl^-, H^+, and OH^-. Figure 2 clearly shows that the approximate solution for the zeta potential based on eq 20 agrees very well with the numerical solution of the full multi-ion model except when C_0 is sufficiently small (ca. 1 mM) and pH is sufficiently small (ca. pH < 3.5) or sufficiently large (ca. pH > 10.5), implying that if C_0 is large and/or pH is in the range of 3.5 < pH < 10.5 the influence of the hydrogen and hydroxyl ions on the zeta potential becomes insignificant. Even though at low (high) level of pH the influence of the H^+ (OH^-) coming from the dissociation of HCl (KOH) and H_2O becomes significant and should not be ignored compared to C_0, the relative error of the zeta potential between these two results is still less than 5%, showing that the approximate model without considering the H^+ and OH^- ions in the evaluation of the net charge density is applicable to the entire pH range of 3–11 under consideration. Figure 2 also depicts that the zeta potential modulated by the FET largely depends on the pH value and the bulk ionic concentration, which are two important parameters in the charge-regulated model. In general, the smaller the C_0 and/or pH, the higher is the magnitude of the zeta potential tuned by the FET, as shown in Figure 2c,d. The former is due to the fact that for higher C_0 the double layer is thinner and more

dx.doi.org/10.1021/jp211496b | J. Phys. Chem. C 2012, 116, 4209–4216

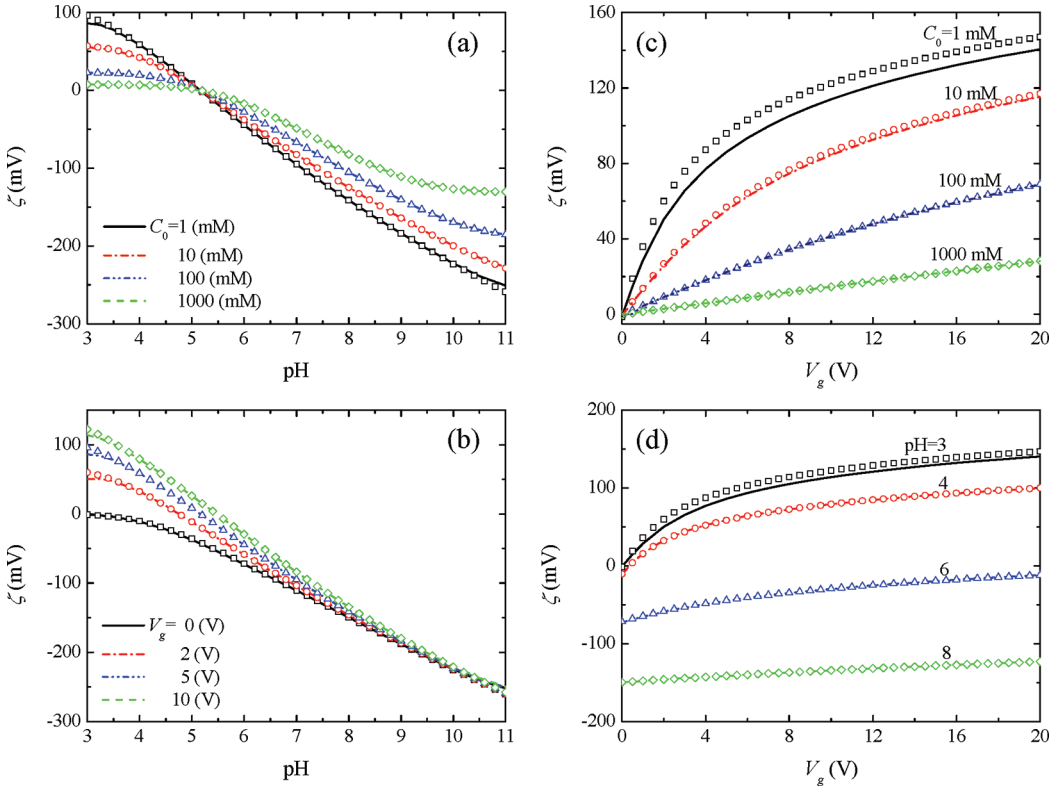

Figure 2. Variations of zeta potential ζ as a function of pH at various combinations of the bulk ionic concentration C_0 and applied gate potential V_g (a) and (b) and as a function of V_g at various combinations of the bulk ionic concentration C_0 and pH (c) and (d). The dielectric layer is made of SiO_2 with δ = 10 nm, ϵ_d = 3.9, $N_{total} = 8 \times 10^{-6}$ mol/m^2, pK_A = 6.8, and pK_B = 1.9. (a) V_g = 5 V, (b) C_0 = 1 mM, (c) pH = 3, and (d) C_0 = 1 mM. Lines and symbols represent, respectively, the results from the full multi-ion model and the approximate model based on eq 20.

counterions are confined within the EDL in the vicinity of the solid/liquid interface, making the FET harder to tune the zeta potential. On the other hand, as pH increases, more negatively charged Si−O$^-$ is dissociated from the functional groups at the interface, resulting in an increase in surface charge density at the interface and accordingly leading to the same behavior as in the case of higher bulk concentration C_0. This implies that the degree of tuning the zeta potential by the FET will be suppressed when pH is relatively high, as clearly shown in Figure 2d. It should be noted that although in the present case the point of zero charge (PZC) is approximately at pH = 2.45 the PZC will be changed when a gate potential is imposed. Figure 2b depicts that PZC increases with increasing V_g in general.

Since the present charge-regulated model is verified to be applicable to the entire pH range of 3−11, we further examine the effects of the applied gate potential, V_g, the bulk ionic concentration, C_0, and the pH of the aqueous solution on the surface charge density of the FET solid/liquid interface, σ_w, based on eq 14. Figure 3 depicts that σ_w is not a constant value but depends largely on the variations of C_0, pH, and V_g. In general, the magnitude of σ_w increases with an increase in pH and V_g and a decrease in C_0. These results clearly show that the basic assumption of a constant surface charge density on the FET solid/liquid interface[17,19−25] is inaccurate and unrealistic and can result in incorrect estimation of electrokinetic phenomena.

The approximate analytical solution for the zeta potential, eq 25, is also validated by comparing its results with those from the already verified implicit eq 20. Figure 4 depicts the zeta

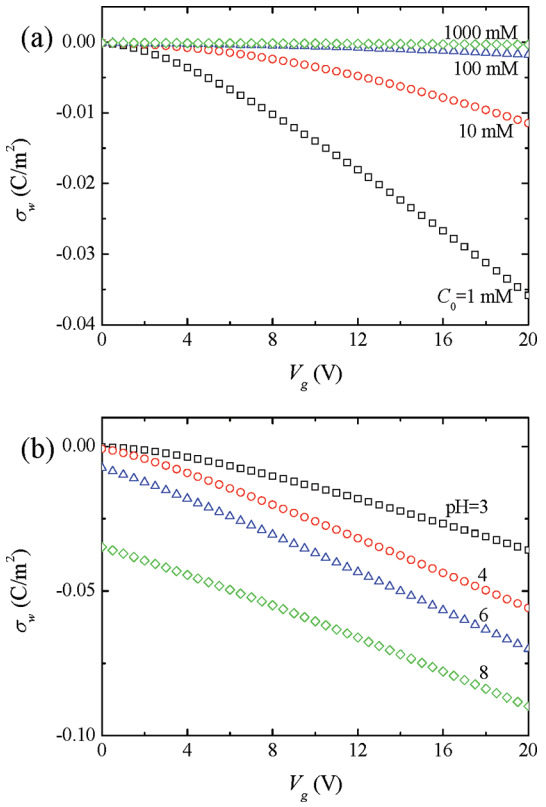

Figure 3. Variations of surface charge density σ_w as a function of the applied gate potential V_g at various values of the bulk ionic concentration C_0 (a) and the pH (b) for the case of Figures 2c and d, respectively.

dx.doi.org/10.1021/jp211496b | J. Phys. Chem. C 2012, 116, 4209−4216

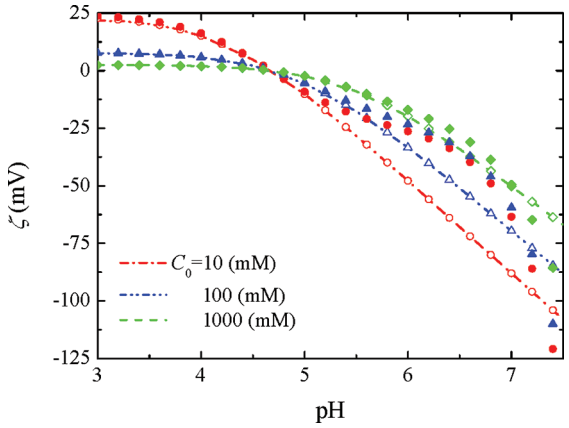

Figure 4. Variations of zeta potential ζ as a function of pH for various values of bulk ionic concentration C_0 when V_g = 5 V, and the dielectric layer is made of SiO_2 with δ = 30 nm, ε_d = 3.9, N_{total} = 8 × 10^{-6} mol/m^2, pK_A = 6.8, and pK_B = 1.9. Lines, open, and solid symbols represent, respectively, the results of the full multi-ion model, the approximate model (eq 20), and the approximate analytical model (eq 25).

potential as a function of pH when the gate potential is V_g = 5 V. The solid and open symbols represent, respectively, the zeta potentials obtained from the closed-form analytical solution (eq 25) and the implicit approximation (eq 20). The lines represent the zeta potential obtained from the full multi-ion model taking into account all four ions. Note that the closed-form analytical solution, eq 25, is only valid when the zeta potential is smaller than the thermal potential, RT/zF = 25.7 mV. Table 1 summarizes the relative percentage deviation

Table 1. Relative Percentage Deviation in the Zeta Potential, RPD (%), for the Approximate Result of the Implicit Equation, Equation 20, (a), and the Approximate Analytical Expression, Equation 25, (b), for the Case of Figure 4

(a)	C_0 (mM)	pH = 3	pH = 5	pH = 7
	10	4.39	0.018	0.003
	100	0.53	0.036	0.019
	1000	0.071	0.053	0.022
(b)	C_0 (mM)	pH = 3	pH = 5	pH = 7
	10	8.97	11.08	27.89
	100	1.04	3.65	14.51
	1000	0.24	0.62	1.42

in the zeta potential, RPD (%), for the case of Figure 4. The RPD is defined as RPD = 100% × $(\zeta - \zeta_{exact})/\zeta_{exact}$, where ζ_{exact} is the zeta potential predicted from the full multi-ion model. An excellent agreement between the approximate results based on eq 20 and the exact numerical results is obtained except when pH and C_0 are sufficiently small, which is consistent with the results shown in Figure 2. The RPD is still less than 5% even when pH and C_0 are relatively low. When the pH exceeds a certain threshold value, the magnitude of zeta potential is above 25.7 mV. As expected, the prediction of the analytical solution, eq 25, significantly deviates from those obtained from the full multi-ion model and the implicit approximation solution when $|\zeta|$ > 25.7 mV. In the range of $|\zeta|$ < 25.7 mV, the predictions from the closed-form model agree with those of the other two models.

Figure 5 depicts the EOF velocity profile for various combinations of the pH value, the bulk ionic concentration,

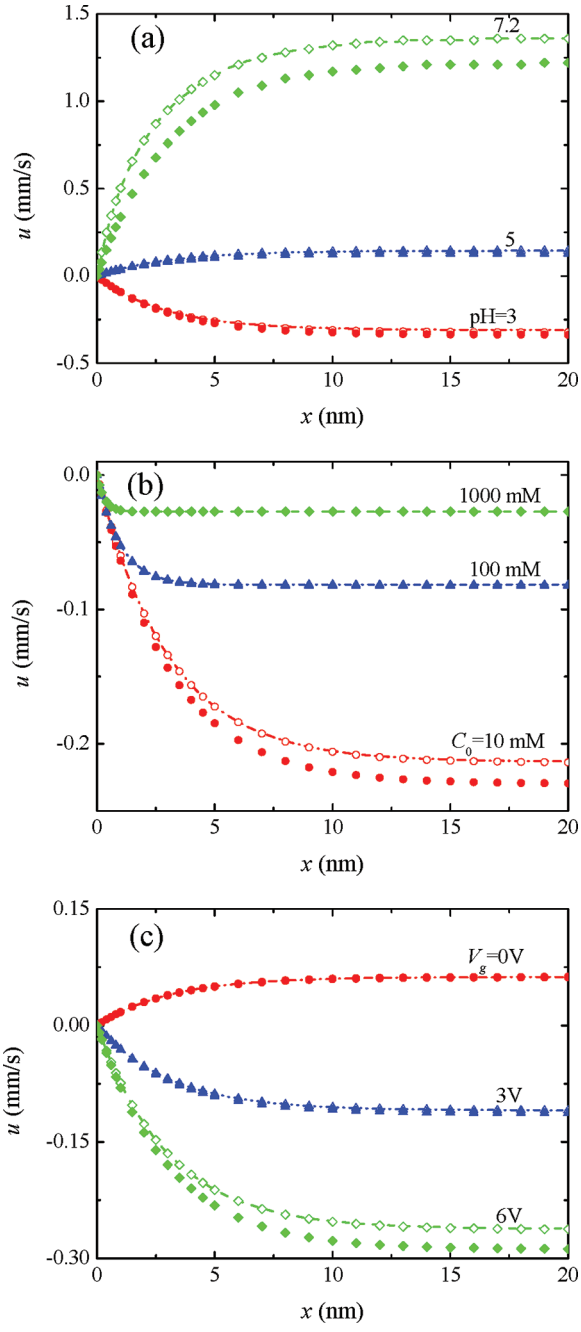

Figure 5. Spatial variations of the EOF velocity driven by E_z = 20 kV/m at various combinations of pH value, bulk ionic concentration C_0, and applied gate potential V_g for the dielectric layer made of SiO_2 with δ = 30 nm, ε_d = 3.9, N_{total} = 8 × 10^{-6} mol/m^2, pK_A = 6.8, and pK_B = 1.9. (a) C_0 = 10 mM and V_g = 5 V, (b) pH = 4 and V_g = 5 V, and (c) C_0 = 10 mM and pH = 4. Lines, open, and solid symbols represent, respectively, the results of the full multi-ion model, the approximate model (eqs 19 and 20), and the approximate analytical model (eqs 23 and 25).

C_0, and the applied gate potential, V_g. The lines, open symbols, and solid symbols represent, respectively, the numerical results from the full multi-ion model based on eqs 1−3, the results of the implicit approximate model based on eqs 19 and 20, and the approximate analytical results based on eqs 23 and 25.

dx.doi.org/10.1021/jp211496b | J. Phys. Chem. C 2012, 116, 4209−4216

The contribution of the ions H^+ and OH^- to the net charge density, ρ_e, is neglected in the approximate model. With the accurate prediction of the zeta potential, the EOF velocity profile predicted from eq 19 agrees with that from the full multi-ion model. Within the range of $|\zeta| < 25.7$ mV, the zeta potential can be accurately predicted by the closed-form model based on eq 25, and accordingly the EOF velocity profile predicted by eq 23 agrees with that from the full model. When $|\zeta| > 25.7$ mV, as in the case of pH = 7.2 in Figure 5a, the case of C_0 = 10 mM in Figure 5b, and the case of V_g = 6 V in Figure 5c, due to significant error in the prediction of the zeta potential from eq 25, the predicted EOF velocity from eq 23 significantly deviates from that obtained from the full multi-ion model.

Figure 5 also indicates that the EOF velocity profile can be modulated by adjusting the values of pH, C_0, and V_g, and the EOF direction can be easily changed by tuning the pH and V_g. The degree of tuning the surface charge property and accordingly the electrokinetic phenomena (i.e., ionic current and EOF) by the FET depends on the properties of the electrolyte (i.e., pH and C_0) and the dielectric layer (i.e., N_{total}, pK_A, and pK_B). The change of other parameters such as N_{total}, pK_A, and pK_B can be achieved by choosing various materials for the dielectric layer[10,23] or conducting appropriated surface modification of that layer.[8,9,12] The choice of the properties of the electrolyte and dielectric layer to achieve the best FET control is an interesting optimization problem, for which the implicit approximation model developed can be very useful.

3.2. Verification of the Model by Experimental Data.

To ensure that the developed implicit approximate model can successfully capture the underlying physics, it is further validated by comparing its predictions to existing experimental data available in the literature. When the FET is inactive (i.e., no gate potential is applied), since the permittivity of the dielectric layer is much smaller than that of the liquid, one can neglect the second term in the left-hand side of eq 6. Following the same derivation described in Section 2.2, we obtain the implicit equation to estimate the zeta potential of a charge-regulated planar surface when the FET is inactive as

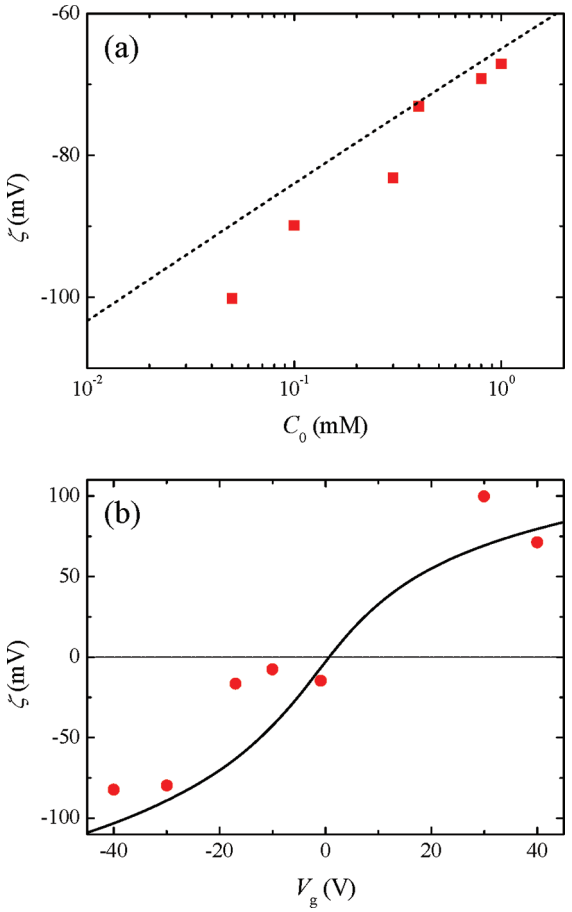

Figure 6. Zeta potential of an isolated flat silica surface as a function of the bulk ionic concentration (a) and zeta potential versus the gate potential in a SiO_2-based nanochannel embedded with a nanofluidic FET (b). Squares in (a) represent the experimental data from Gaudin and Fuerstenau at pH = 6.5,[32] and circles in (b) represent the experimental data of Oh et al.[17]

$$\frac{2\varepsilon_0\varepsilon_f\kappa RT}{zF}\sinh\left(\frac{Fz\zeta}{2RT}\right) = -FN_{total}\left\{\frac{K_A - K_B\left[[H^+]_0\exp\left(-\frac{F\zeta}{RT}\right)\right]^2}{K_A + [H^+]_0\exp\left(-\frac{F\zeta}{RT}\right) + K_B\left[[H^+]_0\exp\left(-\frac{F\zeta}{RT}\right)\right]^2}\right\} \quad (26)$$

Again, one can easily use the Matlab built-in function, *fzero*, to determine the zeta potential for given pH, C_0, and parameters related to the physiochemical properties of the dielectric material. Figure 6a shows the zeta potential of an isolated flat silica surface as a function of the bulk ionic concentration, C_0, at pH = 6.5. The symbols represent the experimental data obtained by Gaudin and Fuerstenau,[32] while the line represents the prediction from eq 26 for $N_{total} = 8 \times 10^{-6}$ mol/m^2, pK_B = 1.9,[31] and pK_A = 7.5.[33] When the FET is inactive, the prediction of the zeta potential of the silica surface is in good agreement with the experimental data for large C_0. It is to be noted that larger deviation between the result predicted by eq 26 and the experimental data[32] is found when C_0 is very small (i.e., <0.3 mM). This might be caused by the fact that for small C_0 the zeta potential can be influenced by other existing ions (i.e., buffer solution). Therefore, our approximate model based on eq 26 successfully captures the charge regulation nature of the charge-regulated surface in general.

When the FET is active, Figure 6b depicts the zeta potential of a gated silica-based nanofluidic device as a function of the gate potential. The symbols represent the experimental data obtained by Oh et al.[17] at pH = 4, C_0 = 1 mM, and the dielectric layer thickness δ = 100 nm. The half width of the nanochannel in the experimental device is about W = 250 nm, which is much larger than the Debye length (i.e., ~9.6 nm), and thus our model is still valid. The line represents the predicted zeta potential based on our implicit model (eq 20) using the typical physiochemical values for silica, $N_{total} = 8 \times 10^{-6}$ mol/m^2, pK_B = 1.9,[31] and pK_A = 7.5.[33] Figure 6b shows that predictions of our model reasonably agree with experimental data. Note that the zeta potential is negative for V_g = 0, which corresponds to the case of an ungated silica nanochannel.

dx.doi.org/10.1021/jp211496b | J. Phys. Chem. C 2012, 116, 4209–4216

4. CONCLUSIONS

A full multi-ion model and an approximate model for analyzing the surface charge property and EOF in gated nanofluidic devices by FET have been developed and validated. In contrast to the existing studies, in which a prespecified constant surface charge density is used, our model takes into account the charge regulation as functions of the properties of the electrolyte solution and the physicochemical properties of the dielectric material. The surface charge density thus is part of the solution instead of being specified externally. All ions are considered in the full multi-ion model, while the contribution of the ions H^+ and OH^- to the charge density is neglected in the approximate model. Approximate expressions, including analytical and implicit ones, have been derived for the first time to estimate the zeta potential and the EOF velocity tuned by the FET. The closed-form analytical model is valid when the magnitude of the zeta potential is less than the thermal potential, while the simple implicit expression agrees with the full multi-ion model in the range of most typical experimental conditions. The implicit approximate model is further validated by comparing its predictions to existing experimental data for the cases of both inactive and active FET. Our results demonstrate that the surface charge property as well as the direction and magnitude of the EOF can be actively tuned by the FET. The degree of FET control is more sensitive when the pH and/or the bulk electrolyte concentration is relatively low. In addition, the degree of controlling the charge property and electrokinetic phenomena also depends on the physicochemical properties of the dielectric material. We believe that the validated implicit model would be very useful for optimizing the FET to control the electrokinetic transport of ions, fluids, and particles in micro/nanofluidic devices. The present model does not consider the EDL overlapping, which will be a subject for future study for a more complete understanding of the field effect.

AUTHOR INFORMATION

Corresponding Author

*E-mail: sqian@odu.edu (Shizhi Qian); jphsu@ntu.edu.tw (Jyh-Ping Hsu).

Author Contributions

[‖]These two authors contributed equally to this work.

Notes

The authors declare no competing financial interest.

ACKNOWLEDGMENTS

This work was financially supported, in part, by the Korea Institute of Machinery & Materials (KIMM), the World Class University Grant No. R32-2008-000-20082-0 of the Ministry of Education, Science and Technology of Korea, and the National Science Council of the Republic of China.

REFERENCES

(1) Li, J.; Stein, D.; McMullan, C.; Branton, D.; Aziz, M. J.; Golovchenko, J. A. *Nature* **2001**, *412*, 166−169.
(2) Storm, A. J.; Chen, J. H.; Ling, X. S.; Zandbergen, H. W.; Dekker, C. *Nat. Mater.* **2003**, *2*, 537−540.
(3) Dekker, C. *Nat. Nanotechnol.* **2007**, *2*, 209−215.
(4) Howorka, S.; Cheley, S.; Bayley, H. *Nat. Biotechnol.* **2001**, *19*, 636−639.
(5) Craighead, H. *Nature* **2006**, *442*, 387−393.
(6) Howorka, S.; Siwy, Z. *Chem. Soc. Rev.* **2009**, *38*, 2360−2384.
(7) Schoch, R. B.; Han, J. Y.; Renaud, P. *Rev. Mod. Phys.* **2008**, *80*, 839−883.
(8) Stein, D.; Kruithof, M.; Dekker, C. *Phys. Rev. Lett.* **2004**, *93*, 035901.
(9) Ali, M.; Ramirez, P.; Mafe, S.; Neumann, R.; Ensinger, W. *ACS Nano* **2009**, *3*, 603−608.
(10) Firnkes, M.; Pedone, D.; Knezevic, J.; Doblinger, M.; Rant, U. *Nano Lett.* **2010**, *10*, 2162−2167.
(11) Horvath, J.; Dolnik, V. *Electrophoresis* **2001**, *22*, 644−655.
(12) Ali, M.; Yameen, B.; Cervera, J.; Ramirez, P.; Neumann, R.; Ensinger, W.; Knoll, W.; Azzaroni, O. *J. Am. Chem. Soc.* **2010**, *132*, 8338−8348.
(13) Schasfoort, R. B. M.; Schlautmann, S.; Hendrikse, L.; van den Berg, A. *Science* **1999**, *286*, 942−945.
(14) Karnik, R.; Fan, R.; Yue, M.; Li, D. Y.; Yang, P. D.; Majumdar, A. *Nano Lett.* **2005**, *5*, 943−948.
(15) Goldberger, J.; Fan, R.; Yang, P. D. *Acc. Chem. Res.* **2006**, *39*, 239−248.
(16) Zhang, Y.; Gamble, T. C.; Neumann, A.; Lopez, G. P.; Brueck, S. R. J.; Petsev, D. N. *Lab Chip* **2008**, *8*, 1671−1675.
(17) Oh, Y. J.; Garcia, A. L.; Petsev, D. N.; Lopez, G. P.; Brueck, S. R. J.; Ivory, C. F.; Han, S. M. *Lab Chip* **2009**, *9*, 1601−1608.
(18) Plecis, A.; Tazid, J.; Pallandre, A.; Martinhon, P.; Deslouis, C.; Chen, Y.; Haghiri-Gosnet, A. M. *Lab Chip* **2010**, *10*, 1245−1253.
(19) Ai, Y.; Liu, J.; Zhang, B. K.; Qian, S. *Anal. Chem.* **2010**, *82*, 8217−8225.
(20) Ai, Y.; Liu, J.; Zhang, B. K.; Qian, S. Z. *Sens. Actuators, B* **2011**, *157*, 742−751.
(21) Jin, X. Z.; Aluru, N. R. *Microfluid. Nanofluid.* **2011**, *11*, 297−306.
(22) Zhang, M. K.; Ai, Y.; Sharma, A.; Joo, S. W.; Kim, D. S.; Qian, S. Z. *Electrophoresis* **2011**, *32*, 1864−1874.
(23) He, Y. H.; Tsutsui, M.; Fan, C.; Taniguchi, M.; Kawai, T. *ACS Nano* **2011**, *5*, 5509−5518.
(24) He, Y. H.; Tsutsui, M.; Fan, C.; Taniguchi, M.; Kawai, T. *ACS Nano* **2011**, *5*, 8391−8397.
(25) Xue, S.; Hu, N.; Qian, S. *J. Colloid Interface Sci.* **2012**, *365*, 326−328.
(26) Sverjensky, D. A.; Sahai, N. *Geochim. Cosmochim. Acta* **1996**, *60*, 3773−3797.
(27) Behrens, S. H.; Grier, D. G. *J. Chem. Phys.* **2001**, *115*, 6716−6721.
(28) Hsu, J. P.; Tai, Y. H. *Langmuir* **2010**, *26*, 16857−16864.
(29) Pennathur, S.; Santiago, J. G. *Anal. Chem.* **2005**, *77*, 6782−6789.
(30) Li, D. *Electrokinetics in Microfluidics*; Elsevier Academic Press: New York, USA, 2004.
(31) Andersen, M. B.; Frey, J.; Pennathur, S.; Bruus, H. *J. Colloid Interface Sci.* **2011**, *353*, 301−310.
(32) Gaudin, A. M.; Fuerstenau, D. W. *Trans. Am. Inst. Min. Metall. Eng.* **1955**, *202*, 66−72.
(33) Hiemstra, T.; Dewit, J. C. M.; Vanriemsdijk, W. H. *J. Colloid Interface Sci.* **1989**, *133*, 105−117.